



Full Length Article

Carbon-dioxide sequestration by mechanical activation of Linz-Donawitz steel slag; the effect of water on CO₂ captureTamás Kurusta^{a,*}, Gábor Mucsi^a, Sanjay Kumar^b, Ferenc Kristály^c^a University of Miskolc, Institute of Raw Material Preparation and Environmental Processing, Miskolc-Egyetemváros, Miskolc HU-3515, Hungary^b National Metallurgical Laboratory India Sunigerya, Burma Mines Colony, Burma Mines, Jharkhand 831001, India^c University of Miskolc, Institute of Mineralogy and Geology, Miskolc-Egyetemváros, Miskolc HU-3515, Hungary

ARTICLE INFO

Keywords:

Mineral carbonation
CO₂ sequestration
Slag waste
Mechanical activation, waste utilization

ABSTRACT

Mineral carbonation, a process of carbon-dioxide (CO₂) captured from the atmosphere or flue gases, is a way to sequester CO₂ safely and permanently. In this technology, CO₂ is chemically reacted with calcium, magnesium, sodium, and iron-containing materials. The procedure is analogous to natural weathering processes, to form thermodynamically stable and environmentally harmless carbonate minerals. Our research was focused on simultaneous mechanical activation and CO₂ capture and storage (CCS) on Linz-Donawitz steel slag dominantly composed of Ca-silicate and oxide phases. The experiments were carried out in a planetary ball mill under 5 bar CO₂ pressure in dry and wet (deionized H₂O) conditions. The primary objective of the experiments was to observe the role of H₂O in the reactions. The presence of H₂O in the system leads to a finer particle size distribution but, at the same time, reduces the number of active sites. H₂O also acts as a carbonate reaction promoter, it is expected to initialize silicate (Windt et al. 2010) surface protonation and enhancing Ca leaching. The latter of the two processes was predominant so that in wet condition (0,246 kgCO₂/kg), almost three times as much calcite is produced as in dry condition (0,083 kgCO₂/kg). The combination of nano milling and wet media carbonation is a promising process to reduce energy requirement through increasing the reaction rate and promotes the use of Ca-silicate wastes otherwise underperforming in CCS.

1. Introduction

Mineral carbonation is one of the feasible methods of CO₂ sequestration. In the process, CO₂ reacts with minerals rich in Ca and Mg prone to form carbonates [53]. Capture by metal-oxides is an exothermal reaction which can be described with the following equation (Eqn. (1)), where MO indicates the metal oxide, for instance, lime (CaO) or periclase (MgO):



For mineral-based CO₂ sequestration, mainly alkaline and alkaline-earth oxides (CaO, MgO; [5] or silicate minerals (olivine, serpentinite, talc, anorthite or albite, according to [29,74,55] are used. The amount of generated heat depends on the starting raw material (olivine: 89 kJ/mol, serpentinite 64 kJ/mol, wollastonite 90 kJ/mol; Zevenhovene et al., 2002). Calcium-rich materials typically have a faster rate of carbonate reaction than magnesium-rich minerals [62]. Also, oxide minerals react

in a significantly shorter time than silicate minerals [15,11]. Following the reactions, CO₂ is present as carbonate (anhydrous, OH⁻ or H₂O bearing) in various forms, such as calcite (CaCO₃), magnesite (MgCO₃) or siderite (FeCO₃), although pressure and temperature highly impacts the reaction rate [37]. Alkali silicates (e.g. feldspars) will generate more complex phases, like dawsonite [NaAlCO₃(OH)₂] [73,11]. The precipitating Mg-phases are also various, like hydromagnesite [Mg₅(CO₃)₄(OH)₂·4H₂O] and hydrotalcite [Mg₆Al₂CO₃(OH)₁₆·4(H₂O)] [66], but mostly related to silicates of ultramafic rocks, with fewer mentions on metallurgical slags. Beyond oxides and silicates, the reactions will also be initiated with cations in phosphate and sulfate frameworks, resulting in structural decomposition and crystallization of new phases [5]. Temperature and pressure affect the solubility of CO₂ in water and the dissolution of Ca and Mg from the solid phase [22]. The two solubilities, in turn, change inversely with increasing temperature. Low temperature favors the water solubility of CO₂, while high temperature favors the water solubility of Ca and Mg, but the effect is only

* Corresponding author at: Institute of Raw Material Preparation and Environmental Processing, Faculty of Earth and Environmental Sciences, Miskolc, Hungary.
E-mail addresses: tamas.kurusta@uni-miskolc.hu (T. Kurusta), gabor.mucsi@uni-miskolc.hu (G. Mucsi), sanjay_kumar_nml@yahoo.com (S. Kumar), ferenc.kristaly@uni-miskolc.hu (F. Kristály).

<https://doi.org/10.1016/j.fuel.2023.128951>

Received 13 March 2023; Received in revised form 5 June 2023; Accepted 7 June 2023

Available online 21 June 2023

0016-2361/© 2023 The Author(s). Published by Elsevier Ltd. This is an open access article under the CC BY-NC-ND license (<http://creativecommons.org/licenses/by-nc-nd/4.0/>).

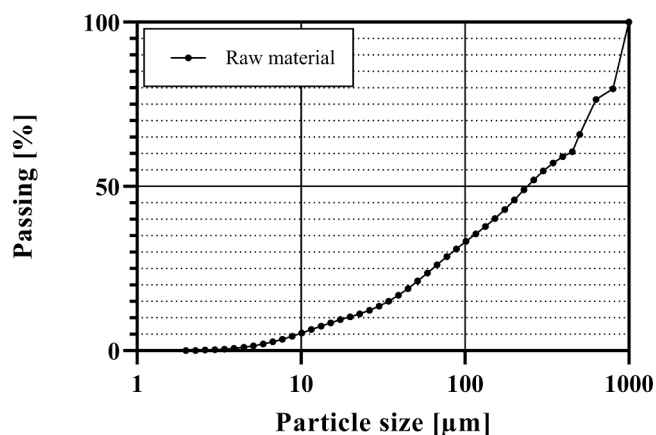


Fig. 1. Particle size distribution of the raw LD slag.

significant at the beginning of the dissolution reaction [30]. The rate of cation extraction from the solid matrix is continuous due to ionic concentration decay by increased carbonate precipitation [31]. The carbonate reaction itself is thermodynamically exothermic, the amount of heat released depends on the metal oxides involved in the process [35]. The optimum temperature for the carbonate reaction is between 30 °C and 70 °C [28,8].

Research in recent years has focused on utilizing the CO₂ sequestration potential of industrial by-products [32], including steel slags [2,54,50], construction and demolition wastes [19,17,27], red mud [52,75,41] and fly ash [60,69,68]. Steel plants continue to be among the high waste generating and high CO₂ emitting industries. Waste utilization and decarbonization are two of the top priorities of steel plants across the world. The global production of steel slag is estimated at 190–280 million tons [45]. A special type of steel slag is the Linz-Donawitz (LD) slag, generated in 150 to 200 kg amount per ton of steel produced, and it has limited utilizations. As LD slag contains a high percentage of calcium oxide, it is considered a potential material for mineral carbonation. LD slag for CO₂ sequestration will be a circular economy approach and provide a dual solution for slag utilization and CO₂ reduction. Theoretical CO₂ sequestration capacity of LD slags is 0.27–0.47 kg CO₂/kg slag [34].

The CO₂ sequestration can be carried out both as in-situ and ex-situ reactions [58]. The in situ method is very close to underground storage, with the difference that the reservoir rock will react with the injected CO₂ [16] to form carbonates. The ex-situ process is carried out on mining wastes or industrial by-products, with the requirement of chemical reactors. Therefore, the advantage of the method is that the reactions can be controlled by adjusting all the parameters relevant to the sequestration to the optimal conditions. There are three routes to sequester CO₂: direct gas–solid carbonation [65], direct aqueous carbonation [59,9], and indirect aqueous carbonation [63,76]. Direct carbonate reactions are those processes where suitable Ca- and/or Mg-containing materials are directly reacted with CO₂. Indirect carbonation uses electrolytic solutions to capture CO₂ and obtain carbonate precipitate. Among the direct methods there are single-step (solid + CO₂ reactions) and multi-step (chemical cation extraction for solution + CO₂ reactions) procedures [58,18]. One of the most important physical parameters controlling the overall evolution of carbonation is the specific surface area of the capturing agent [23,14], determined by particle size, thus adjustable by mechanical processing.

In this research work, the Linz-Donawitz (LD) slag-based CO₂ sequestration was investigated through silicate carbonation promoted by mechanical activation. The aim of the experiments is CO₂ capture and sequestration (CCS) in stable form by mineral carbonation. We have used the direct carbonation method, where the reactivity of the slag was increased by high-energy milling in dry and wet media. Mechanical activation by dry milling generates reactive particle surfaces, expected to increase carbonation reaction rate [64]. On the other hand, it has been experimentally proven, that the presence of H₂O molecules also increases carbonation [20], and initialize silicate surface protonation and enhancing Ca leaching [72]. To reduce the surface reactivity and increase the agglomeration stability during mechanical activation, grinding aids are used to produce fine and ultrafine grinds [10], and water also plays a similar role in wet grinding. The novelty of our experiments is the combination of mechanical activation by wet milling coupled with carbonation and the results support the benefits of the process versus dry milling and other CCS techniques. However, even at the laboratory scale system design the issue of captured/emitted CO₂ balance asks for discussion, for which we offer details together with the discussion of reactions and quantitative approach of CCS.

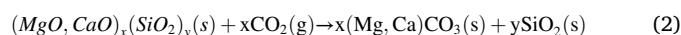
2. Processes and reactions

The primary limiting factors of industrial-scale ex-situ direct CO₂ sequestration based on mineral carbonation include high energy demand (milling, mechanical activation), low mineral conversion rates (temperature dependent), and extended reaction time. Conversion rate and reaction time are negatively influenced by to the formation of a carbonate coating and the presence of a passive silicate layer [71]. A common method for CCS is the direct, single step procedure, to bring the suitable feedstock in direct contact with gaseous or water-dissolved CO₂. Also, this is the case when the passive surface layers have the highest impact, raising the need for mitigation by chemical (solvents) or physical (milling) processes.

The principal processes influencing the reactivity of solid particles are [33,46], and the mineral conversion rate is limited by the slowest of these processes listed below:

- surface kinetics: includes adsorption of the reactant on the surface, surface reactions and desorption of the product into the gas or the liquid phase.
- pore diffusion resistance: how deep the reactant can penetrate into the pores and the solid particles.
- the hydrolysis rate on the surface of the particles, the transport processes in a liquid film.

The initial solid + gas chemical reaction (Eq. (1)) is the most cost-effective option. However, reaction rates will be slow, times are long. The thermodynamic limitation of the process is the high pressure required [21,53] to overcome passivation. The general equation of the chemical reaction on silicates (Eq. (2)) written in theoretical form, is [46]:



Carbonation in solution is a more promising way for single-step sequestration of CO₂, since it can achieve a higher degree of carbonation relatively quickly, but it costs 40–80 € to sequester 1 ton of CO₂ in this way [38]. Under wet conditions, three main reactions occur in the reactor [23,39]. The first (Eqs. (3) and (4)) is the dissolution of CO₂ in

Table 1

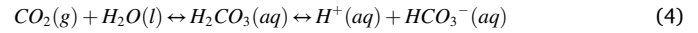
Oxidic components of LD slag (weight percent, error +/- 0.01 relative percent, LOI 3.95 wt%).

| SiO ₂ | Al ₂ O ₃ | MgO | CaO | Na ₂ O | K ₂ O | Fe ₂ O ₃ | Mn ₂ O ₃ | TiO ₂ | P ₂ O ₅ | SO ₃ | P | ZnO |
|------------------|--------------------------------|------|-------|-------------------|------------------|--------------------------------|--------------------------------|------------------|-------------------------------|-----------------|------|------|
| 13,05 | 2,74 | 5,11 | 45,06 | 0,05 | 0,02 | 25,48 | 0,69 | 0,97 | 2,5 | 0,35 | 0,02 | 0,01 |

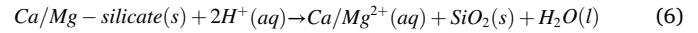
Table 2
Mineral components of the raw LD slag (wt%, error +/−1 relative%).

| Phase | Dolomite CaMg(CO ₃) ₂ | Srebrodolskite Ca ₂ Fe ₃ ²⁺ O ₅ | Brownmillerite Ca ₂ (Al _{1.1} Fe _{0.9} O ₅) | Bredigite; Ca ₇ Mg(SiO ₄) ₄ | Portlandite; Ca (OH) ₂ | Larnite; Ca ₅ SiO ₄ | Lime CaO | Sellaite MgF ₂ | Quartz SiO ₂ | Wuestite Fe ²⁺ O | Ilmenite Fe ²⁺ TiO ₃ | Iron alpha α-Fe | Fluorite CaF ₂ | Amorphous |
|-------|---|--|---|--|--------------------------------------|--|-------------|------------------------------|----------------------------|--------------------------------|---|-----------------------|------------------------------|-----------|
| Raw | 1.4 | 14.1 | 9.9 | 1.7 | 0.6 | 26.7 | 5.8 | 0.5 | 0.6 | 12.3 | 0.1 | 0.4 | 1.1 | 24.8 |

water to produce carbonic acid. Hydrogen ions are then dissociated from the carbonic acid, forming bicarbonate and ultimately carbonate ions, easily reacting with cations.



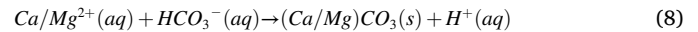
Cations, preferably Ca and Mg can enter the reactions in several ways. Firstly, the pH of the resulting solution will drop to slightly acidic (5–5.5), favorable for leaching of cations. On the other side, Ca and Mg on the free surface of crystal grains will be affected by hydrolysis reactions initiated by H⁺ (Eq. (6)):



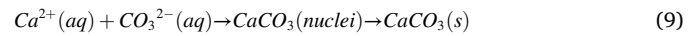
Cation release may also happen into a surface hydrated layer, not only as a bulk solubilization. In addition to the process described in Eq. (6), the dissolved Ca²⁺ and Mg²⁺ is converted into hydroxide phase. The calcium from the hydroxide phase [Ca(OH)₂] will not precipitate in the absence of other radicals, but it dissociates into Ca²⁺ and OH[−] as follows:



This also prevents the precipitation of Mg(OH)₂, or other cations, generating the reactive electrolyte. Finally, the dissolved calcium and magnesium reacts with the dissolved bicarbonate and precipitates as a carbonate mineral (Eqs. (8) and (9)):



In the systems with high Ca concentration Eq. (9) becomes dominant, the final product being calcite, able to take up also solubilized Mg²⁺:



In direct aqueous systems, the rate of carbonation is predominantly limited by the dissolution rate of minerals. This can be increased using additives or adjusting the process temperature, CO₂ concentration and pressure, solid to liquid ratio, and particle size [77]. Thus, coupling carbonate reactions with milling (dry or wet) and adjustable CO₂ pressure is expected to be beneficial to reduce the negative passivation effect of inert silica (SiO₂) layers, and the formed carbonate coating surface will be less prevalent.

3. Material and methods

3.1. Raw material

The experiments were carried out on Linz-Donawitz (LD) steel slag from Tata Steel, Jamshedpur (India). The feed slag was previously subjected to a two-stage particle size reduction in jaw crusher, followed by hammer crusher with 1 mm mesh size. The resulted particle size distribution (determined with LPSA, see 3.3) is shown in Fig. 1, displaying a median size of 238 μm. The initial moisture content (laboratory oven, 105 °C, 3x10 g samples) was found to be 0.65 wt%, while the loss on ignition (Nabertherm B 180 furnace, 950 °C with 120 min soaking, 3x1 g samples) is 2.56 wt%. The slag has a particle density ρ = 3.32 g/cm³ and a bulk density ρ = 1.82 g/cm³. Research grade (99.5%) Biogon-C CO₂ gas was used for the sequestration tests without further purification.

Composition of starting material was determined for oxides (XRF, see 3.3.) and minerals (XRD, see 3.3.). The oxidic composition of the raw slag is shown in Table 1. The major component of the slag is CaO, proving it a suitable material for CCS. Other major components are Fe₂O₃ SiO₂, with an additional significant amount of MgO and Al₂O₃ (Table 1.). The results are consistent with previous chemical analysis by other researchers [48,1,51].

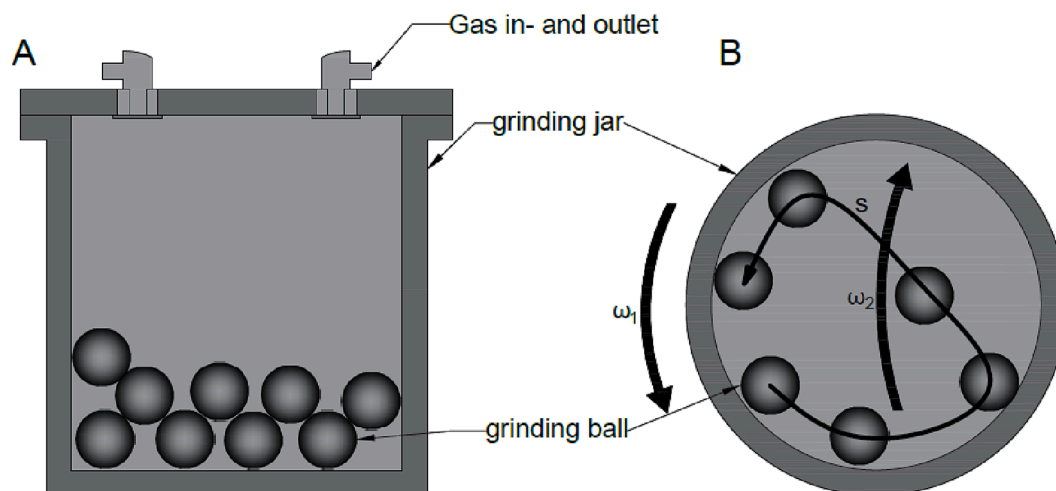


Fig. 2. Schematic diagram of the grinding jar serving as the reaction chamber. A: side view; B: top view (ω_1 : rotation direction of the grinding jar, ω_2 : rotation direction of the sun disc, s: the path of the grinding balls)

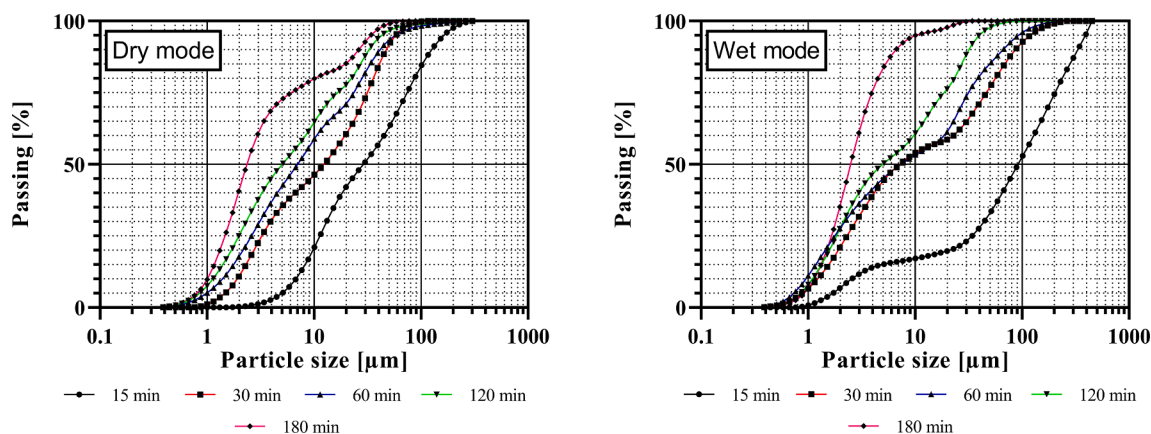


Fig. 3. Particle size distribution of slag ground under dry and wet conditions.

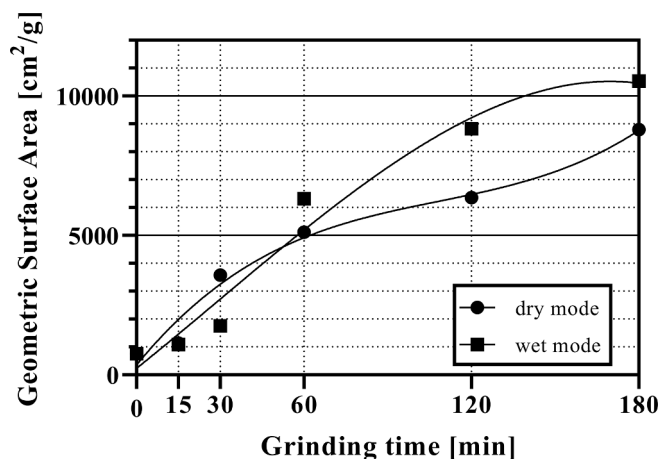


Fig. 4. The geometric surface area of the milled slag.

The crystalline phases constituting the slag are shown in Table 2. In addition to the silicates from the slag former (28,8 wt%), the sample also contains a significant amount of metal oxide minerals (42,8 wt%) and a 24,8 wt% amorphous fraction.

The crystalline phases of the slag are in accordance with the chemical analysis and most of them is expected to be reactive in CCS processes: srebrodolskite, brownmillerite, bredigite, portlandite, larnite, lime., The

amorphous fraction, based on the balance of XRF and XRD results, is mostly oxidic with $\text{Ca} > \text{Fe} > \text{Mg}$ composition, but LOI values indicate the presence of carbonate or hydrated components also. Fluorite is the residue of fluxing agent from melting.

3.2. Mechanical activation and ccs

During the experiments, mechanical activation and CO_2 sequestration were performed simultaneously in a Fritch Pulverisette 5 planetary ball mill, under wet and dry conditions. The milling was carried out using 500 ml steel jars and grinding media (Fig. 2). The jars were filled with 54.3 g of dry sample and 543 g of 30 mm diameter grinding balls. During wet condition experiments, 162.9 g of deionized H_2O was added to the same solid amount in the grinding jar and balls. The rotation speed of the sun disk was 200 rpm, the shift between the sun disk and the grinding jars was 1:2. The operating parameters of the mill were based on empirical considerations. To initiate carbonate reactions, the jars were flooded with CO_2 at 5 bar, after filling the slag and water. In order to ensure the necessary CO_2 for the reactions, the jars were sequentially refilled by each 15 min, to reach the initial CO_2 pressure.

3.3. Characterization of reaction products

The change in dispersity was determined with a Horiba-La-950 V2 laser particle size analyzer (LPSA) in suspension using deionized H_2O as dispersing media. For better dispersion of fine particles, before the

Table 3The results of the EDX analyses of the raw LD slag sample (wt%, error ± 0.5 relative%).

| | Pic | Nr | MgO | SiO ₂ | CaO | Cr ₂ O ₃ | MnO | FeO | Al ₂ O ₃ | P ₂ O ₅ | TiO ₂ | SO ₂ | Na ₂ O |
|----------------|-----|----|-------|------------------|-------|--------------------------------|------|-------|--------------------------------|-------------------------------|------------------|-----------------|-------------------|
| α -Fe | A | 6 | | | 0.69 | | | 99.31 | | | | | |
| Wüstite | A | 7 | 6.24 | | 7.94 | | 0.58 | 85.23 | | | | | |
| Mg-wüstite | B | 1 | 29.74 | | 1.09 | 0.51 | 1.78 | 66.88 | | | | | |
| | B | 3 | 29.74 | | 1.25 | 0.58 | 2 | 66.43 | | | | | |
| | B | 4 | 27.84 | | 2.95 | 0.57 | 1.78 | 66.86 | | | | | |
| | C | 1 | 28.47 | | 2.41 | | 2.1 | 67.02 | | | | | |
| | C | 4 | 28.91 | | 1.99 | | 2.17 | 66.94 | | | | | |
| | K | 4 | 44.55 | | 1.22 | 0.61 | 1.26 | 52.36 | | | | | |
| Srebrodolskite | A | 3 | 0.66 | 1.14 | 47.96 | 0.37 | | 33.25 | 9.46 | | 7.16 | | |
| | B | 2 | 0.77 | | 49.11 | | | 32.49 | 14.42 | | | | |
| | B | 5 | 1.07 | 2.09 | 46.04 | 0.74 | 0.1 | 30.1 | 10.99 | 0.93 | 7.95 | | |
| | C | 2 | 0.88 | 0.89 | 45.37 | 3.17 | 0.13 | 38.75 | 5.4 | | 5.41 | | |
| | C | 3 | 0.82 | 0.81 | 45.75 | 2.42 | 0.32 | 38.76 | 5.36 | | 5.77 | | |
| | F | 1 | 6.95 | 5.47 | 32.73 | 0.41 | 1.42 | 43.99 | 5.44 | 1.52 | 2.07 | | |
| | F | 2 | 7.53 | 7.8 | 32.58 | 0.34 | 1.51 | 41.56 | 5.29 | 1.41 | 1.98 | | |
| | I | 1 | | 1.42 | 45.56 | | | 41.35 | 4.37 | | 7.31 | | |
| | K | 2 | 0.66 | 0.99 | 45.96 | 0.45 | | 39.58 | 6.33 | | 6.03 | | |
| | K | 3 | 0.76 | 0.84 | 45.87 | 1.13 | | 41.19 | 4.18 | | 6.04 | | |
| | J | 1 | 0.7 | 2.12 | 46.16 | 0.43 | | 34.84 | 7.17 | | 8.58 | | |
| | J | 2 | 0.56 | 1.26 | 46.24 | 0.16 | | 37.83 | 7.45 | | 6.49 | | |
| Brownmillerite | D | 4 | 1.77 | | 43.81 | | | 0.68 | 53.18 | | | 0.56 | |
| | D | 5 | 1.34 | 1.55 | 56.41 | | | 0.29 | 40.42 | | | | |
| | D | 6 | 1.36 | 1.97 | 56.88 | | | | 39.79 | | | | |
| | H | 2 | 0.94 | 0.82 | 43.88 | | 1.24 | 1.25 | 50.36 | | | 1.52 | |
| | K | 1 | 0.53 | 3.68 | 55.48 | | 1.52 | 1.22 | 37.57 | | | | |
| | L | 1 | 0.86 | | 44.03 | | | 0.04 | 55.07 | | | | |
| Bredigite | K | 5 | 1.8 | 15.51 | 77.63 | | | 2.72 | 0.98 | 0.98 | | 0.38 | |
| Larnite | C | 5 | 0.75 | 57 | 27.42 | | 0.08 | 4.05 | 7.77 | 2.41 | 0.31 | 0.21 | |
| | J | 3 | 1.89 | 43.58 | 30.37 | | | 12.05 | 2.5 | 9.09 | 0.52 | | |
| Cebollite | E | 3 | 7.79 | 35.75 | 36.35 | | | | 19.35 | | | 0.33 | 0.44 |
| | E | 1 | 7.6 | 35.04 | 36.34 | | | | 20.71 | | | 0.31 | |
| | I | 2 | 7.56 | 33.61 | 37.07 | | | | 21.77 | | | | |

measurement, sodium pyrophosphate was added to the samples, applying ultrasonic stirring for one minute. The particle size distribution (PSD) was estimated by Fraunhofer's approximate method from the measured data, while geometric surface area (GSA), as a parameter related to external or relative surface area, obtained by software-based calculation from the PSD data assuming a spherical particle surface [26]. Even if the obtained data is not comparably with BET specific surface area, it is a useful measure for system dispersivity.

Wavelength dispersive X-ray fluorescence (WD-XRF) measurement was performed using a Philips Axios PW 4400/24 type WD-XRF, analytical range from Be to U. The radiation source was a rhodium (Rh) X-ray tube with an excitation voltage of 2,4 kV. The samples were prepared by melting in a 1/8 sample/melt weight ratio $\text{Li}_2\text{B}_4\text{O}_7/\text{LiBO}_2$ (lithium-tetraborate/lithium-metaborate) solvent.

Scanning electron microscopy and energy dispersive spectrometry (SEM + EDX) were carried out on the raw slag materials, on epoxy resin embedded polished specimen with a carbon coating layer. Measurements were done on a Jeol JXA 8600 Superprobe with W-filament (20 kV acceleration voltage, 20nA probe current), recording back-scattered electron images (BSE). Chemical analysis for selected phases was measured by standardless EDX with Si-drift detector, 60 sec counting time, quantified with PAP correction.

X-ray Powder Diffraction (XRD) was used to identify and characterize LD slag sample before and after CO_2 sequestration with a Bruker D8 Advance diffractometer using $\text{Cu K}\alpha$ radiation (40 kV, 40 mA) in parallel beam geometry obtained with Göbel mirror, in the 2θ range

(2θ) range with a 0.007° (2θ) step interval and a 24 s step counting time. The Bruker DiffracPlus software package was used to identify the crystalline phases, in its EVA module, using ICDD PDF-2 (2005) database for search/matching of phases. The quantitative evaluation was carried out by Rietveld refinement in TOPAS4 software, where the amorphous content was determined by the amorphous hump method.

4. Results

4.1. Grain size evolution during the experiments

The size of the particles that make up the slag significantly impacts CO_2 sequestration. As the particle size decreases, the reactive surface area of the sample material and the amount of material involved in the reactions increases [6]. However, in the simultaneous milling-reacting experiments, both mechanical and chemical processes are involved in dispersity evolution, without a strict boundary.

By examining the particle size distribution curves (Fig. 3), in the first 15 min of milling finer particle size is achieved with the dry method. In the absence of fluid phase, particles cannot avoid the milling media, therefore a higher probability of fragmentation arises. However, in the 15–30 min period the fine grain production decreases, in contrast to wet milling, while after 60 min the median particle sizes (D_{50}) of dry ($92 \pm 2 \mu\text{m}$) and wet ($86 \pm 2 \mu\text{m}$) milling are very similar. In further milling, a finer particle size distribution is achieved by wet method,

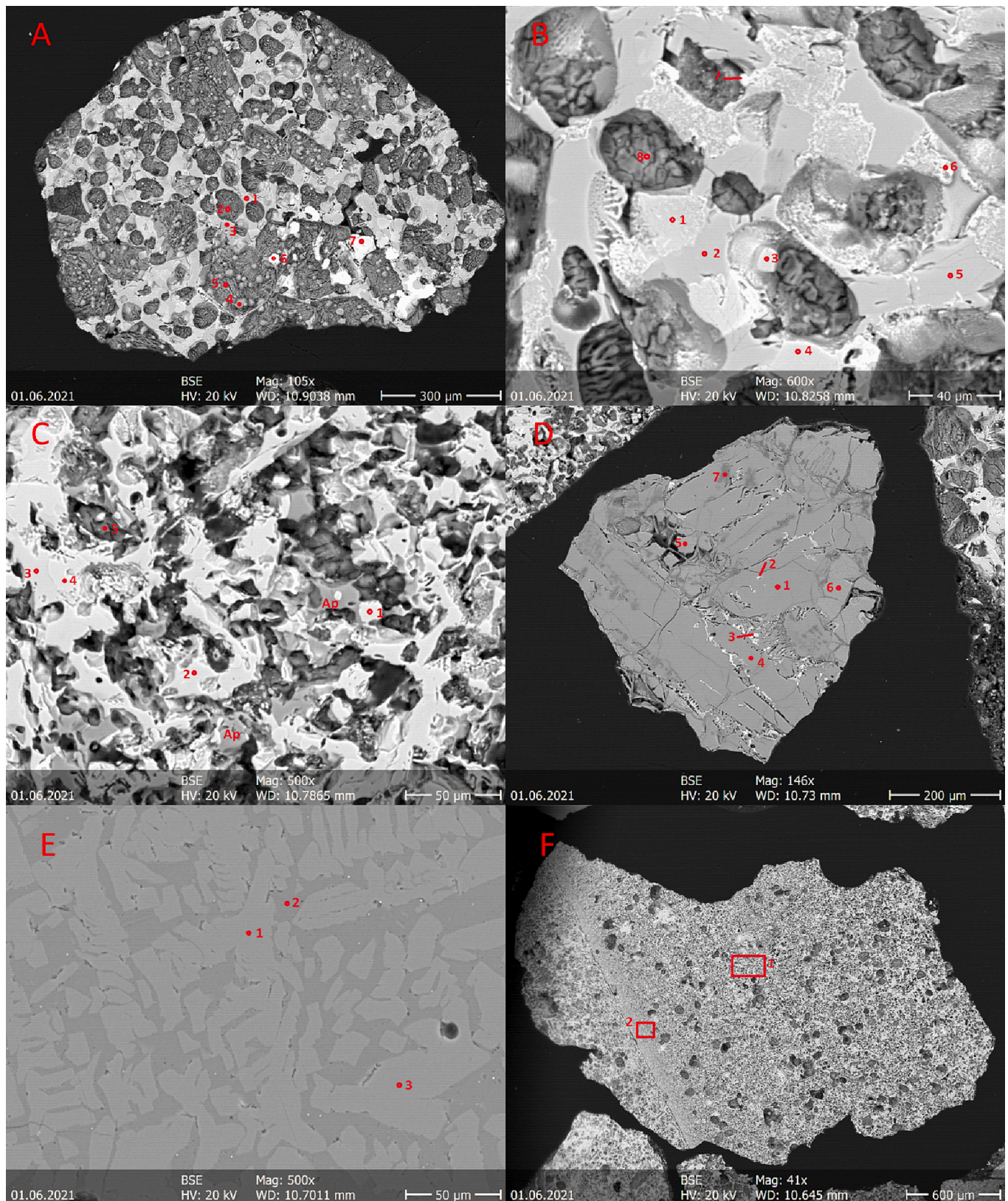


Fig. 5. The morphology of the raw LD slag sample, numbers with dots or rectangles indicate the EDX measurement spots (see Table 3).

because the slip effect of the covering liquid layer starts to dominate, and this prevents the particles from aggregating.

In dry milling, the median particle size decreases monotonically in the first 60 min, followed by a plateau until 120 min, and then a decrease

again in the last hour, but less than the initial decrease. In the first 15 min of wet milling, the median particle size shows only a minor decrease, significantly less than in dry milling.

This divergence can be observed in the change of GSA evolution

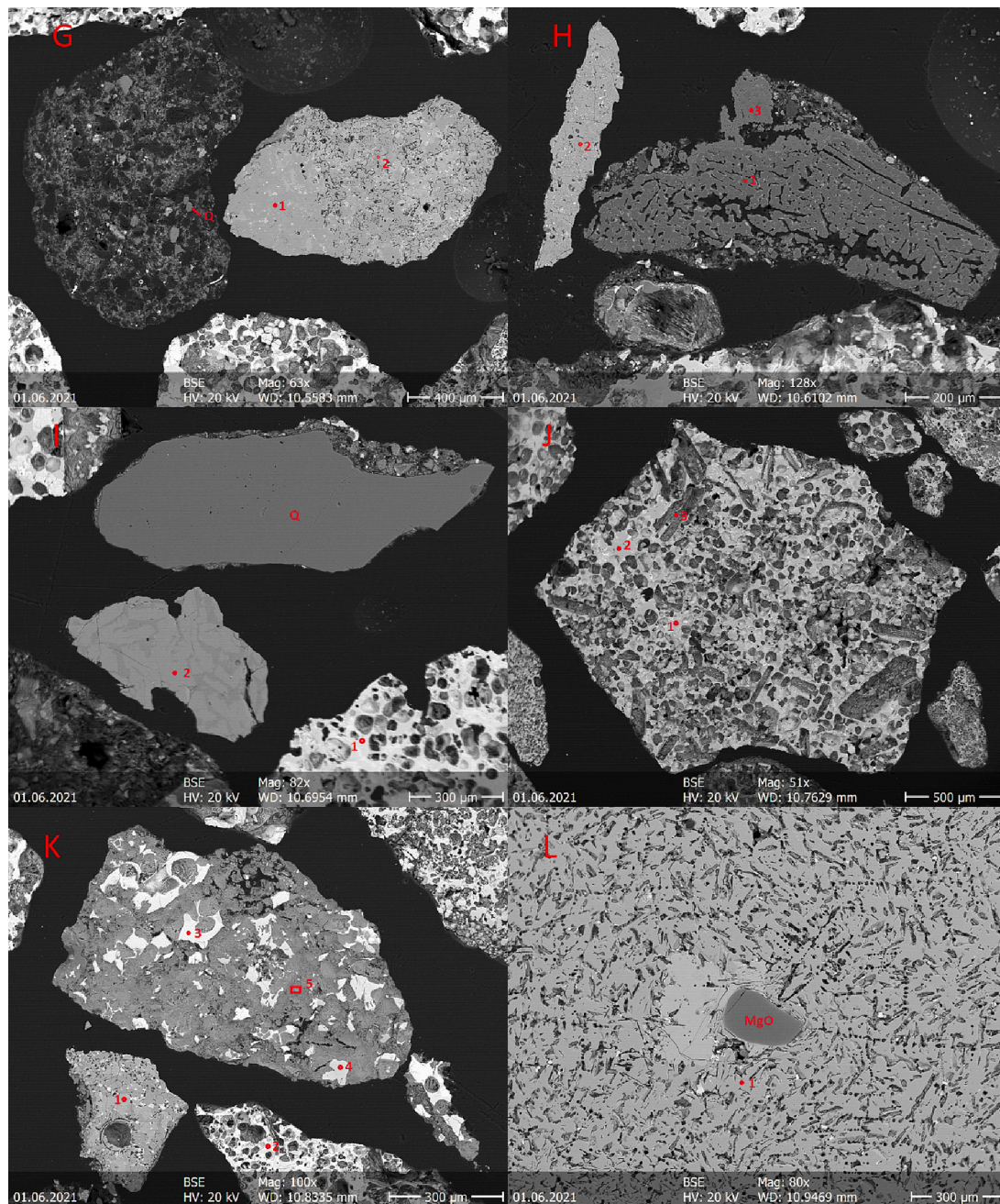


Fig. 6. The morphology of the raw LD slag sample, numbers with dots or rectangles indicate the EDX measurement spots (see Table 3).

(Fig. 4). A higher surface area is obtained after 30 min in dry conditions ($3600 \text{ cm}^2/\text{g}$), two times higher than in wet conditions ($1700 \text{ cm}^2/\text{g}$). After that, for the reason described above, the geometric surface area of the wet milled sample ($10500 \text{ cm}^2/\text{g}$) becomes 1.2 times greater than in the dry condition ($8700 \text{ cm}^2/\text{g}$). Based on the GSA curves, it is also possible to determine the specific stages of the milling process [44]. The Rittinger stage is recognized by the rapid increase in GSA, in our case lasts 30 min in dry milling and 60 min in wet conditions. The 2nd stage of milling is the aggregation stage, in the wet setting it lasts from 60 min to the end, while in the dry setting is observed between 30 and 60 min. According to general milling theory, the last stage is the agglomeration [3], dominated by decrease or stagnation of GSA stage. However, in our experiments this stage is eliminated by the carbonation reactions, leading to continuous abrasion.

4.2. Mineral characteristics and structural changes

The mineralogical composition was determined by XRD, comparing the results with bulk chemical analysis by XRF. Both methods show that the LD slag is Ca-rich, mainly silicate-based material. SEM + EDS investigation of at least the raw slag was necessary to successfully interpret phase changes by XRD, dissolution, and crystallization. The identified crystalline phases were accepted only after confirmation by SEM + EDX. Due to the rapid decrease of particle size, this method was not suitable to investigate the milled samples.

4.3. Slag phases susceptible in ccs

Figs. 3 and 4 show the phase distribution in the particles of the LD slag. The BSE images confirm that the starting material is composed of particles smaller than 1 mm, which correlates with the particle size

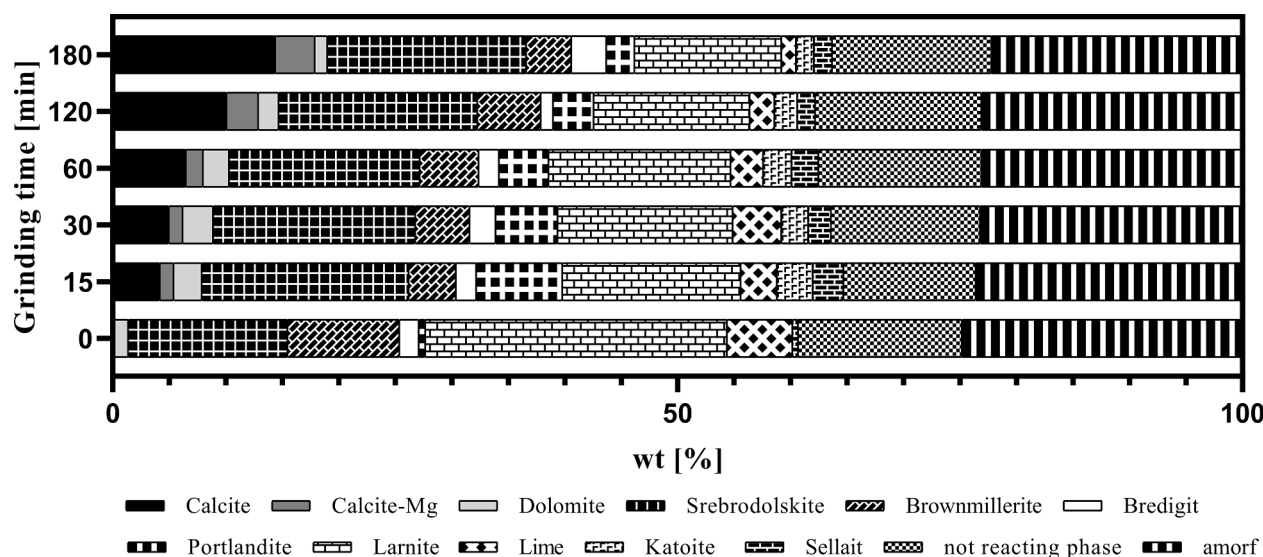


Fig. 7. Effect of grinding time on CO₂ sequestration in dry conditions.

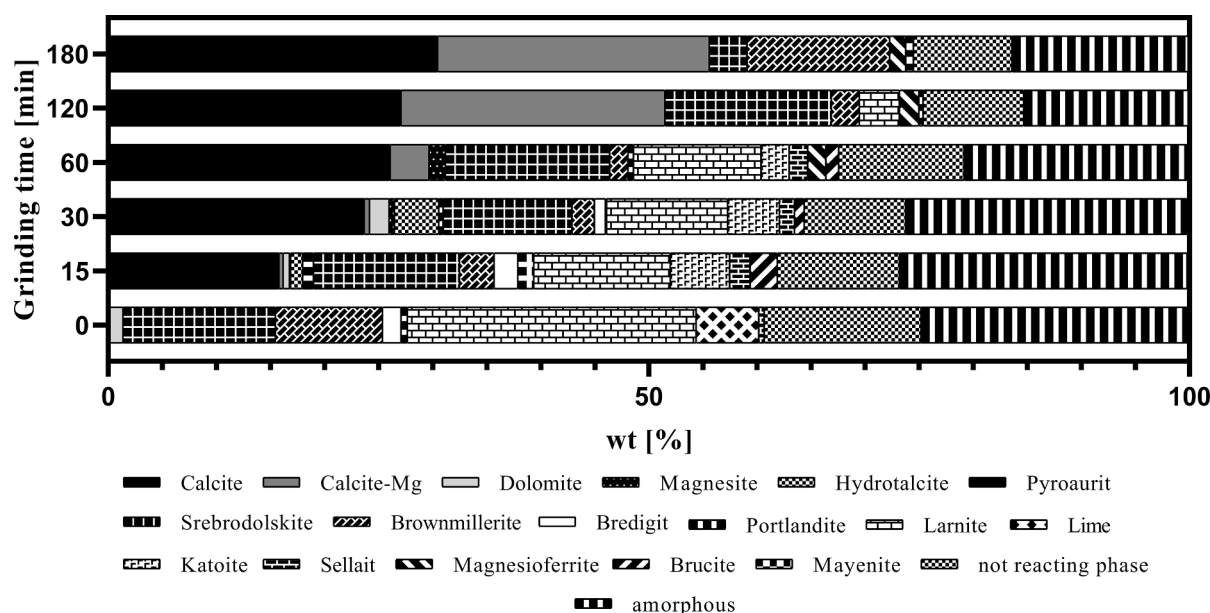


Fig. 8. Effect of grinding time on CO₂ sequestration in wet conditions.

distribution and screening. The slag phases are various in chemical composition and texture but can be correlated to the XRD results.

The EDX measurements are summarised in Table 3, and the BSE images are shown in Figs. 4 and 5. The α -Fe phase by XRD, also known as ferrite, is present in 10–50 μ m grains. As the main constituent of cast iron and steel, it is the leftover from steel production. Fig. 6.

Some small areas in the matrix have magnesioferrite (MgFe_2O_4) composition, in which magnesium is slightly replaced by calcium, but since this phase was not observed by XRD, we assume it to be Mg-wüstite [56], less likely amorphous. These phases are the high-temperature oxidic product of slag formation, expected to react in CCS due to Ca and Mg content. The XRD results are grouped as wüstite, which matches the actual chemical composition.

The major Ca-bearing phases are Ca-ferrite and aluminate compositions, corresponding to the srebrodolskite-brownmillerite solid-solution series. The srebrodolskite ($\text{Ca}_2\text{Fe}_2\text{O}_5$) chemical composition comprises ~15% iron with ~5% magnesium, chromium, and manganese substituents, reflected by the crystal structure refined by Rietveld

refinement. The brownmillerite ($\text{Ca}_2(\text{Al,Fe})_2\text{O}_5$) is iron-deficient compared to the empirical composition ($\text{Al}_{1.1}\text{Fe}_{0.9}$), presumably due to metallurgical processes. It contains magnesium, silicon, and manganese as contaminant elements. The EDX measurements show that the slag contains a higher amount of srebrodolskite from the srebrodolskite-brownmillerite series.

Confirmation of the presence of bredigite ($\text{Ca}_7\text{Mg}(\text{SiO}_4)_4$) in the sample is made by EDX. The measurements suggest that silicon is slightly substituted for phosphorus and is also present in microcrystalline inclusions. Magnesium is substituted by iron, and some other elements are also impurities.

Also shown is a metastable mineral phase, larnite (Ca_2SiO_4). Several common impurity elements are observed by EDX: magnesium, manganese, iron, aluminum, phosphorus, and titanium.

Cebollite ($\text{Ca}_5\text{Al}_2(\text{SiO}_4)_3(\text{OH})_4$) is also found to be present in the sample. Cebollite in nature occurs as an alteration product of melilite in carbonatites. A thermodynamic simulation of steel slag crystallization indicated that the melilite forms as the last phase during crystallization

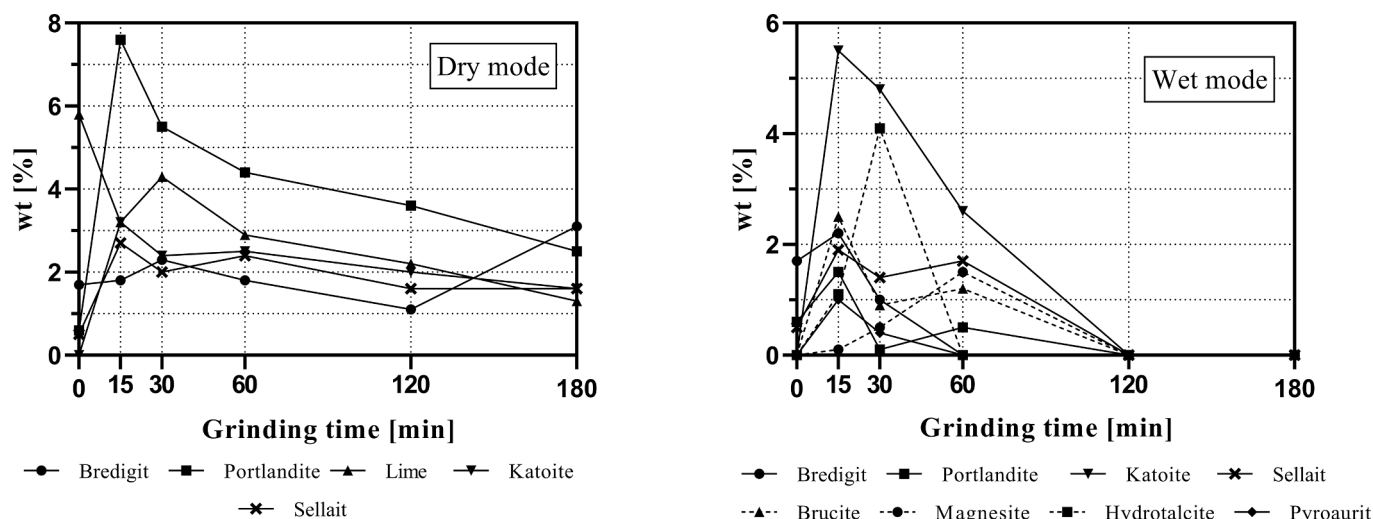


Fig. 9. Change in the ratio of reactive phases.

[42]. The measured results show a 20% substitution between calcium and magnesium and the presence of typical ceboillite-like contaminants such as potassium and sodium. Although XRD does not identify this phase, it is known as a slag component.

Lime (CaO) and portlandite Ca(OH)_2 , are the most reactive phases with CO_2 , not observed by SEM + EDX due to their probable alteration during specimen preparation, but these were detected by XRD measurement.

4.4. Carbonation products by xrd and rietveld refinement

Figs. 7–9 and Table 4 show the results of the two capture experiments. Two main carbonate phases are formed, pure calcite and calcite with magnesium content. In both cases, it is observed that calcite is formed first, followed by the formation of only calcite-Mg.

The most significant decrease after CO_2 is applied is measured for larnite and lime, and the SiO_2 released from larnite decomposition precipitates as amorphous silica. Towards the end of the milling, the ratio of these two phases decreases to the greatest extent, being completely reacted in wet grinding, while in dry grinding, their ratio decreases by 1/2. In both cases, the proportion of srebrodolskite and brownmillerite also decreases. After 180 min, the reduction was 3/10 in dry grinding and 1/10 in wet grinding. Different behavior is observed for bredigite, which does not react with CO_2 under dry conditions but reacts entirely at the end of the milling in the presence of H_2O . Five mineral phases in the slag (quartz, wuestite, ilmenite, iron alpha, and the fluorite) did not react with the added CO_2 , these phases are shown as non-reacting phase in the Figs. 7 and 8.

Fig. 9 Shows the changes in the minor phases that can sequester CO_2 . Two of the minerals (portlandite and katoite), in both conditions show an increase from the initial state in the first 15 min. However, these only become visible by XRD after the amount of major phases decreases due to the carbonation, which results in decreased peak overlapping on the XRD patterns. On the other hand, portlandite might be the reaction of CaO with residual air moisture.

Significant differences appear between the two milling conditions, mostly in calcite production, but also in the hydrated phases. Mg carbonates containing water [hydrotalcite, $\text{Mg}_6\text{Al}_2\text{CO}_3(\text{OH})_{16}\cdot 4(\text{H}_2\text{O})$; pyroaurite, $\text{Mg}_6\text{Fe}_2^{3+}(\text{CO}_3)(\text{OH})_{16}\cdot 4(\text{H}_2\text{O})$] would be formed in the first 30 min under wet conditions. These disappear after 30 min, and with them appears the Mg-containing calcite.

A difference is observed also for the phases that can react with CO_2 under normal conditions: lime and portlandite partially react in dry conditions, but other susceptible minerals (bredigite, srebrodolskite,

brownmillerite) do not react with CO_2 . Under wet conditions, in contrast, the lime, portlandite and bredigite react, and 3/10 of the srebrodolskite-brownmillerite reacts with CO_2 .

The polynomial curve in Fig. 10. shows the total amount of carbonate phases the proportion increasing differently with the reaction time. It reaches only 19 wt% after 180 min for dry grinding, whereas in wet setting it reaches 56 wt%. Furthermore, the curve almost plateaus after 15 min in dry milling. In contrast, wet milling shows a reduced steepness for 30–60 min and flattens after 120 min, giving the optimum reaction time. Based on the XRD measurement, the temporal position of the plateau coincides with the point from which the formation of Mg-containing calcite dominates over pure calcite.

The formation and dominance of Mg-calcite in the second part of the milling is due to the delayed dissolution of Mg-phases, mainly bredigite. Although Mg-calcite formation is elevated, the Mg content is very low based on the XRD peak positions [61]. Since Mg dissolution rate can be high, the precipitation rate of carbonate phase is low [47], thus Mg carbonate was not produced. In contrast, the Mg^{2+} ion is well absorbed on the surface of calcite crystallites, from which it is incorporated into the lattice [4,12]. The general chemical formula of Mg-bearing calcite is $(\text{Ca}_{1-x}\text{Mg}_x)\text{CO}_3$, where $0,1 < x < 0,25$ [61]. It can incorporate more Mg than in the equilibrium state, but this will reduce the rate of calcite crystal formation [4]. Examining the Mg-bearing slag phases decomposition, this may partly explain the flattening in the carbonation rate between 30 and 60 min, the release of Mg temporarily reduces calcite precipitation. After equilibration of Mg^{2+} on the surface of existent calcite crystal nuclei, carbonate formation is reinitiated.

5. Discussion

During mechanical activation, beyond size decrease also the number of defects in the crystal lattice increases, leading to amorphous fraction increase [3,40]. In our simultaneous milling an CO_2 input experiments, however, the amorphous components are also consumed by carbonation as shown by XRD results. The carbonated products are continuously removed from particle surfaces as suggested by the rapid increase of fine fraction, creating fresh reactive surfaces for mechanical activation and carbonation. The abrasion of carbonated surfaces is supported by both continuous particle size decrease and GSA increase, in contrast with general milling practice. These processes all contribute to an increase in CO_2 that can be bound. Beyond increased dispersity, the significantly higher carbonation during the wet setting indicates that the presence of H_2O is important also in the chemical reactions, not only as milling media. Thus, a discussion of dominant reactions is also necessary.

Table 4
The results of the quantitative evaluation of XRD on raw and treated LD slag sample (wt%, error +/-1 relative%).

| Phase | CalciteCaCO ₃ | Calcite – Mg(Ca _{0.9} Mg _{0.1})CO ₃ | DolomiteCaMg(CO ₃) ₂ | MagnesiteMgCO ₃ | HydrotalciteMg ₆ Al ₂ CO ₃ (OH) ₁₆ •4(H ₂ O) | PyroauriteMg ₆ Fe ₂ ³⁺ (CO ₃)(OH) ₁₆ •4(H ₂ O) | SrebrodolskiteCa ₂ Fe ₂ ³⁺ O ₅ | Bredigite: Ca ₇ Mg(SiO ₄) ₄ BrownmilleriteCa ₂ (Al _{1.1} Fe _{0.9} ²⁺ O ₅ | Portlandite: Ca(OH) ₂ | Larnite: Ca ₂ SiO ₄ | LimeCaO | KatoiteCa ₃ Al ₂ (SiO ₄) _{1.5} (OH) ₆ | SellaiteMgF ₂ | MagnesianferriteMgFe ₂ ³⁺ O ₄ | BruciteMg(OH) ₂ | QuartzSiO ₂ | WuestiteFe ²⁺ O | IlmeniteFe ²⁺ TiO ₃ | Ironalphase – Fe | FluoriteCaF ₂ | MayeniteCa ₁₂ Al ₁₄ O ₃₃ | amorphous |
|----------|--------------------------|---|---|----------------------------|---|---|--|--|----------------------------------|---|---------|---|--------------------------|--|----------------------------|------------------------|----------------------------|---|------------------|--------------------------|---|-----------|
| Raw | | | 1.4 | | | | 24.0 | 1.7 | 0.6 | 26.7 | 5.8 | | 0.5 | | | 0.6 | 12.3 | 0.1 | 0.4 | 1.1 | | 24.8 |
| Dry mode | | | | | | | | | | | | | | | | | | | | | | |
| 15 min | 4.2 | 1.2 | 2.5 | | | | 22.5 | 1.8 | 7.6 | 15.8 | 3.2 | 3.2 | 2.7 | | | 0.5 | 9.8 | 0.2 | 0.3 | 1 | | 23.6 |
| 30 min | 5 | 1.2 | 2.7 | | | | 22.7 | 2.3 | 5.5 | 15.5 | 4.3 | 2.4 | 2 | | | 0.3 | 11.2 | 0.1 | 0.3 | 1.2 | | 23.2 |
| 60 min | 6.5 | 1.5 | 2.3 | | | | 22.1 | 1.8 | 4.4 | 16.1 | 2.9 | 2.5 | 2.4 | | | 0.8 | 12.2 | 0.1 | 0.3 | 1 | | 23.1 |
| 120 min | 10.1 | 2.8 | 1.8 | | | | 23.2 | 1.1 | 3.6 | 13.8 | 2.2 | 2 | 1.6 | | | 0.2 | 13.1 | 0.1 | 0.3 | 0.9 | | 23.1 |
| 180 min | 14.4 | 3.5 | 1.1 | | | | 21.6 | 3.1 | 2.5 | 13 | 1.3 | 1.6 | 1.6 | | | 0.4 | 12.7 | 0.1 | 0.3 | 0.5 | | 22.1 |
| Wet mode | | | | | | | | | | | | | | | | | | | | | | |
| 15 min | 15.8 | 0.4 | 0.6 | 0.1 | 1.1 | 1 | 16.7 | 2.2 | 1.5 | 12.6 | | 5.5 | 1.9 | | 2.5 | 0.5 | 9.3 | 0.4 | 0.1 | 1 | | 26.6 |
| 30 min | 23.7 | 0.5 | 1.8 | 0.5 | 4.1 | 0.4 | 14.0 | 1 | 0.1 | 11.2 | | 4.8 | 1.4 | | 0.9 | 0.3 | 8.1 | 0.2 | 0.1 | 0.7 | | 26 |
| 60 min | 26.1 | 3.6 | | 1.5 | | | 16.9 | | 0.5 | 11.8 | | 2.6 | 1.7 | | 1.2 | 1 | 9.4 | | 0.2 | 1 | | 20.8 |
| 120 min | 27.1 | 24.4 | | | | | 18.0 | | | 3.7 | | | | 1.8 | | 1 | 7.4 | | 0.3 | 0.6 | 0.4 | 15.2 |
| 180 min | 30.5 | 25.1 | | | | | 16.7 | | | | | | | 1.5 | | 1.1 | 7.5 | | 0.3 | 0.2 | 0.7 | 16.3 |

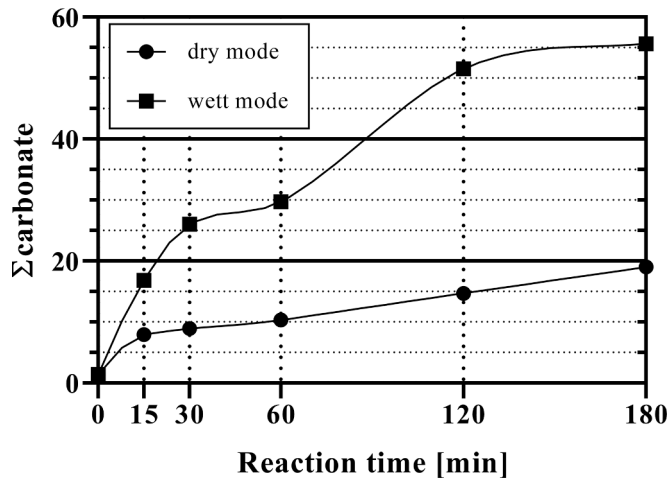


Fig. 10. Changes of carbonate content in measurements under dry and wet conditions.

Solid with gas and solid with solution reactions are initiated only if certain physico chemical conditions appear. Whether the process takes place depends on the free enthalpy of the system (ΔG), which can be calculated with the general formula (Eq. (11)):

$$\Delta G = \Delta H^\circ - T\Delta S^\circ \quad (11)$$

where, in:

- ΔH° is the change of enthalpy [joule].
- T is the temperature [kelvin].
- ΔS° is the change of entropy [joule/kelvin].

If $\Delta G > 0$, the process will not take place; if $\Delta G < 0$, the process will take place. Carbonation, in its simplest form, when metal oxide (MgO, CaO) and hydroxide (Mg(OH)₂, Ca(OH)₂) react with carbon dioxide to form magnesite (MgCO₃) or calcite (CaCO₃), depending on the starting material, proceeds as follows:

Magnesium-oxide



$$\Delta G = -1111,69 \text{ kJ} - 293 \text{ K}^* (65,84 - (26,94 + 213,8)) \text{ J/K} = -65,3 \text{ kJ/K} \quad (13)$$

Even if our slag did not contain periclase (MgO), the Mg on the crystallite surfaces (e.g. Mg-wüstite) is expected to react according to Eq. (12), but magnesite crystallization is prevented by the presence of abundant Ca, leading to Mg-bearing calcite formation on the contacting crystallite surfaces.

Calcium-oxide (lime)



$$\Delta G = -1207,6 \text{ kJ} - 293 \text{ K}^* (91,7 - (31,8 + 213,8)) \text{ J/K} = -131,8 \text{ kJ} \quad (15)$$

This reaction is approximately valid for all Ca-bearing phases, since CaO environment is present on the surface of silicate and oxide phases also. The high reaction rate is observed even in the absence of H₂O

molecules, however in the wet setting further intermediate reactions will accelerate the carbonation processes. The generation of Mg-hydroxide is even observed by XRD at the beginning of wet milling.

Magnesium-hydroxide (brucite):



$$\Delta G = -((1111,7 + 285,8) - (924,5 + 393,5)) \text{ kJ} - 293 \text{ K}^* ((65,8 + 69,1) - (56,2 + 213,8)) \text{ J/K} = -40,0 \text{ kJ} \quad (17)$$

Its later disappearance coincides with the enhanced Mg-bearing calcite generation and depletion of Mg-bearing phases, accelerated by the hydroxide mediated Ca carbonation (Eq. (18)), where both Ca and Mg hydroxides are generated on crystallite surfaces, resulting in leaching and consequent carbonate precipitation.

Calcium-hydroxide (portlandite):



$$\Delta G = -((1207,6 + 285,8) - (986,1 + 393,5)) \text{ kJ} - 293 \text{ K}^* ((91,7 + 69,1) - (83,4 + 213,8)) \text{ J/K} = -73,9 \text{ kJ} \quad (19)$$

While direct carbonation of Ca from the larnite lattice is also possible (Eq. (20)), supported by our XRD results also, the hydrolysis and leaching by hydroxylation promotes the Ca extraction.

Larnite:



$$\Delta G = -((2*1207,6 + 910,9) - (2307,5 + 2*393,5)) \text{ kJ} - 293 \text{ K}^* ((2*91,7 + 41,8) - (127,7 + 2*213,8)) \text{ J/K} = -135,7 \text{ kJ} \quad (21)$$

From the above reaction, larnite transformation is the most important in our case, the stable end product being calcite. The formation rate of calcite in wet and dry mode highlights the role of H₂O as chemical reagent, acting as a proton source according to Eqs. (3) to (6), accelerating hydrolysis and cation leaching. While grain size reduction in the first 15 min has 1/2 ratio for dry/wet setting, the produced calcite is 1/5 for the same ratio, and differences remain significant during the whole experiment. Compared to Eqs. (12) and (16), discordance is observed in the behavior of Mg and its products, as magnesite is produced only in the wet setting, in parallel to brucite, suggesting that Mg is extracted from bredigite and amorphous material by the surface protonation. In contrast, the dry setting produced Mg-bearing calcite instead, the probable product of in-situ carbonation of both Ca and Mg containing materials. The appearance of hydrotalcite in the wet setting is a result of Al leaching from brownmillerite.

Among the anhydrous carbonates, the dissolution of Fe-containing minerals (srebrodolskite, brownmillerite and wüstite) could still produce iron-carbonate. But the formation of siderite would require high temperatures and pressures (>100 °C; >30 bar; [37]). The Fe that enters the system, together with the uncarbonated Mg, forms magnesioferrite (MgFe₂³⁺O₄) minerals, according to the XRD. The crystallization of magnesioferrite is initiated by the oxidation of Fe²⁺ from the wüstite lattice, leaching of Mg and the energy transferred from the milling media

Table 5

A chemical composition of crystalline and amorphous fraction.

| | SiO ₂ | Al ₂ O ₃ | MgO | CaO | Na ₂ O | K ₂ O | Fe ₂ O ₃ | Mn ₂ O ₃ | TiO ₂ | P ₂ O ₅ | SO ₃ | P | ZnO | Total |
|-------------------|------------------|--------------------------------|------|-------|-------------------|------------------|--------------------------------|--------------------------------|------------------|-------------------------------|-----------------|------|------|-------|
| XRF [wt%] | 13,05 | 2,74 | 5,11 | 45,06 | 0,05 | 0,02 | 25,48 | 0,69 | 0,97 | 2,50 | 0,35 | 0,02 | 0,01 | |
| Crystalline [wt%] | 10,52 | 2,31 | 0,73 | 33,32 | | | 8,28 | 0,00 | 0,05 | | | | | 75,20 |
| Amorphous [wt%] | 2,53 | 0,43 | 4,38 | 11,74 | 0,05 | 0,02 | 33,88 | 0,69 | 0,92 | 2,50 | 0,35 | 0,02 | 0,01 | 24,80 |

(mechanochemical transformation).

The maximum capacity of CO₂ that can theoretically be sequestered can be calculated from the oxide product of the components of the slag using the Stenoir's stoichiometric formula (Eq. (10)); [43].

$$\text{CO}_2(\%) \approx 0,785(\% \text{CaO} - 0,7\% \text{SO}_3) + 1,09\% \text{MgO} + 0,71\% \text{Na}_2\text{O} + 0,468\% \text{K}_2\text{O} \quad (10)$$

Based on the LD slag used in the XRF measurements, theoretically assuming all available oxides react to form carbonates, the sequestration capacity of LD slag, for instance, is 40,79%. Therefore, using 1 kg of slag an amount of 0,408 kg of CO₂ can be sequestered. Under our experimental parameters, 1 kg of slag could sequester 0,246 kg of CO₂ under wet conditions and 0,083 kg under dry conditions. This means we could use 3/5 part of the theoretical capacity in wet conditions and 1/5 part in dry conditions. The result obtained is almost equivalent to the amount of CO₂ sequestered (0,296–0,337 kgCO₂/kg) by direct carbonation calculated [49]. The 54.3 g of slag loaded into the mill sequesters 0,022 kgCO₂, with an investment of 0.19 kWh of electricity. This represents an average of 0,046 kgCO₂ emissions in the European Union International Energy Agency [25]. But by scale up and switching to a conventional ball mill, the method can potentially reduce CO₂ emissions.

A special component of starting material is the amorphous phase, or phases, for which the direct reactions cannot be observed by XRD, however its carbonation is evident by the decreasing total amount. A chemical composition of amorphous fraction can be estimated by calculating oxidic composition from the XRD phases, which is then subtracted from the XRF results (Table 5). As a result, we have a dominantly Ca-based material, with significant Si, Mg, Fe and P content. It is the elevated Ca content which makes the amorphous fraction susceptible to carbonation, accelerated by the presence of water.

Compared to similar research, it is observed that in wet mode the time required for carbonation can be greatly reduced with mechanical activation. Nearly the same rate of carbonation can be achieved under wet conditions without mechanical activation, but the reaction time can be up to 240 h [76]. Reducing the reaction time to 40 h also reduces the carbonation rate to 1/2 [7]. The reaction time can be significantly reduced to 120 min by using ammonia salt solutions, with decrease in the carbonation degree to 1/2 [57].

In the dry conditions, significant improvements can be achieved with mechanical activation. Based on measurements with [78], the carbonation degree can be increased from 1/12 to 1/6 with a reaction time of 120 min. The primary cause of the improvement is the fresh fracture surface that is continuously generated during milling.

Our work and other reports show that nearly 50 times more CO₂ can be sequestered in the slag by different slag treatment processes than if it were passively carbonated ((0,296–0,337 kgCO₂/kg; [51]). Therefore, many possibilities to improve the low carbonation degree are feasible. The reaction time can be effectively reduced (without reducing the reaction rate) by direct carbonation within mechanical activation or by indirect methods [24,70].

Possible application of the treated slag in the construction industry, in the production of metallurgical slag cement. Cement produced by the addition of slag is cement with a moderate initial, high final strength, and low tendency to crack and shrink [67]. However, its applicability is limited by the slag's reactive Ca, and Mg content [36], which can be reduced by CO₂ sequestration. Future research plans include applicability investigations.

6. Conclusions

Based on the research results, it can be concluded that CO₂ is bound as calcite and Mg-calcite in the final product. After the tests were carried out, the sample material contained 19% carbonate phases in dry and 56% in wet conditions. In wet conditions, nearly three times as much CO₂ can be sequestered compared to dry one.

The XRD data of the experiments endorses the hypothesis that high energy milling will increase the rate of carbonation. Also, the combined effect of mechanical activation and protonation further accelerates carbonate crystallization on a silicate basis.

Those phases that react with CO₂ under normal conditions (lime, portlandite, larnite) react completely with CO₂ when wet grinding is used. Similarly, these phases reacted partially (lime and portlandite ~60%, larnite ~20%) under dry conditions. For phases that are not reactive under normal conditions, there are variations by mineral. Brownmillerite and srebrodolskite were partially reacted in both measurements, but a 7.5-fold increase (~30% wet, ~4% dry) can be achieved under wet conditions. Bredigite behaves differently, reacting completely with CO₂ under wet conditions but not with CO₂ under dry conditions.

Mechanical activation increases the free surface area, creates a fresh fracture surface, and can produce lattice defects, increasing the reactivity. If water is added to the system during mechanical activation (wet milling), the number of active sites is reduced, but the water will also act as a catalyst. Thermodynamically, the system will change, and as a consequence, CO₂ sequestration under wet conditions will be more advantageous.

CRediT authorship contribution statement

Tamás Kurusta: Writing – review & editing, Writing – original draft, Visualization, Methodology, Conceptualization. **Gábor Mucsi:** Writing – review & editing, Supervision, Project administration. **Sanjay Kumar:** Resources. **Ferenc Kristály:** Writing – review & editing, Supervision, Investigation.

Declaration of Competing Interest

The authors declare that they have no known competing financial interests or personal relationships that could have appeared to influence the work reported in this paper.

Data availability

Data will be made available on request.

Acknowledgments

The cross-cutting research was conducted at the University of Miskolc as part of the „More efficient exploitation and use of subsurface resources” project implemented in the framework of the Thematic Excellence Program funded by the Ministry of Innovation and Technology of Hungary (Grant Contract reg. nr.: NKFIH-846-8/2019), and within the subsequent „Developments aimed at increasing social benefits deriving from more efficient exploitation and utilization of domestic subsurface natural resources” project supported by the Ministry of Innovation and Technology from the National Research, Development and Innovation Fund according to the Grant Contract issued by the National Research, Development and Innovation Office (Grant Contract reg. nr.: TKP-17-1/PALY-2020).

The research was partly funded by the Sustainable Development and Technologies National Programme of the Hungarian Academy of Sciences (FFT NP FTA).

The authors gratefully acknowledge Materials Research and Testing Laboratory for Silicate Industry Ltd., who provided to the research by analysing the chemical composition of the slag.

References

- [1] Ashrit S, Banerjee PK, Ghosh TK, Rayasam V, Nair UG. Characterisation of LD slag fines by X-ray Diffraction. *Metall Res Technol* 2015;112:502. <https://doi.org/10.1051/metall/2015030>.

- [2] Baciocchi R, Costa G, Bartolomeo ED, Polettini A, Pomi R. Carbonation of Stainless Steel Slag as a Process for CO₂ Storage and Slag Valorization. *Waste Biomass Valoriz* 2010;1:467–77. <https://doi.org/10.1007/s12649-010-9047-1>.
- [3] P. Baláz (2008): *Mechanochemistry in Nanoscience and Minerals Engineering*. Springer ISBN: 978-3-540-74855-7.
- [4] Berner RA. The role of magnesium in the crystal growth of calcite and aragonite from sea wat. *Geochim Cosmochim Acta* 1974;39:489–94. [https://doi.org/10.1016/0016-7037\(75\)90102-7](https://doi.org/10.1016/0016-7037(75)90102-7).
- [5] Berner RA, Lasaga AC, Garrels RM. The carbonate-silicate geochemical cycle and its effect on atmospheric carbon dioxide the past 100 million years. *Am J Sci* 1983; 283:641–83. <https://doi.org/10.2475/ajs.283.7.641>.
- [6] Bohács K, Fajtli J, Bokányi L, Mucsi G. Control of natural zeolite properties by mechanical activation in stirred media mill. *1046 Arch Metall Mater* 2017;62: 1399. <https://doi.org/10.1515/amm-2017-0216>.
- [7] Bonenfant D, Kharoune L, Sauvė S, Hausler R, Niquette P, Mimeault M, et al. CO₂ Sequestration Potential of Steel Slags at Ambient Pressure and Temperature. *Ind Eng Chem Res* 2008;47(20):7610–6.
- [8] Chang EE, Chen CH, Chen YH, Pan SY, Chiang PC. Performance Evaluation for Carbonation of Steel-Making Slags in a Slurry Reactor. *J Hazard Mater* 2011;186: 558–66. <https://doi.org/10.1016/j.jhazmat.2010.11.038>.
- [9] Chen Z, Li R, Zheng X, Liu J. Carbon sequestration of steel slag and carbonation for activating RO phase. *Cem Concr Res* 2021;139:106271. <https://doi.org/10.1016/j.cemconres.2020.106271>.
- [10] B. Csőke, Á. Rácz, G. Mucsi. (2010): Grinding and Flowing Investigation on Dry Stirred Ball Milling in Order to Determine the Influence of Grinding Aid. XXV International Mineral Processing Congress: Smarter Processing for the Future. 629–635.
- [11] Dai Z, Xu L, Xiao T, McPherson B, Zhang X, Zheng L, et al. Reactive chemical transport simulations of geologic carbon sequestration: Methods and applications. *Earth Sci Rev* 2020;208:103265. <https://doi.org/10.1016/j.earscirev.2020.103265>.
- [12] Davis KJ, Dove PM, De Yoreo JJ. The Role of Mg²⁺ as an Impurity in Calcite Growth. *Science* 2000;290:1134–7. <https://doi.org/10.1126/science.290.5494.1134>.
- [14] Eloneva S, Said A, Fogelholm CJ, Zevenhoven R. Preliminary Assessment of a Method Utilizing Carbon Dioxide and Steelmaking Slags to Produce Precipitated Calcium Carbonate. *Appl Energy* 2012;90:329–34. <https://doi.org/10.1016/j.apenergy.2011.05.045>.
- [15] Gaus I. Role and impact of CO₂–rock interactions during CO₂ storage in sedimentary rocks. *Int J Greenhouse Gas Control* 2010;4:73–93. <https://doi.org/10.1016/j.ijggc.2009.09.015>.
- [16] Goff F, Lackner KS. Carbon dioxide sequestering using ultramafic rocks. *Environ Geosci* 1998;5:89–101. <https://doi.org/10.1046/j.1526-0984.1998.08014.x>.
- [17] Ghacham AB, Pasquier LC, Cecchi E, Blais JF, Mercier G. Valorization of waste concrete through CO₂ mineral carbonation: Optimizing parameters and improving reactivity using concrete separation. *J Clean Prod* 2017;166:869–78. <https://doi.org/10.1016/j.jclepro.2017.08.015>.
- [18] He M, Teng L, Gao Y, Rohani S, Ren S, Li J, et al. Simultaneous CO₂ mineral sequestration and rutile beneficiation by using titanium-bearing blast furnace slag: Process description and optimization. *Energy* 2022;248:123643. <https://doi.org/10.1016/j.energy.2022.123643>.
- [19] Huntzinger DN, Gierke JS, Sutter LL, Kawatra SK, Eiseled TC. Mineral carbonation for carbon sequestration in cement kiln dust from waste piles. *J Hazard Mater* 2009;168:31–7. <https://doi.org/10.1016/j.jhazmat.2009.01.122>.
- [20] Huijgen WJJ. Carbon dioxide sequestration by mineral carbonation. The Netherlands: Energy research Centre of the Netherlands; 2007.
- [21] Huijgen WJJ, Comans RNJ. Carbon dioxide sequestration by mineral carbonation. Literature Review Energy research Centre of the Netherlands ECN-C-03016 2003.
- [22] Huijgen WJJ, Witkamp GJ, Comans RNJ. Mineral CO₂ Sequestration by Steel Slag Carbonation. *Environ Sci Tech* 2005;39(24):9676–82. <https://doi.org/10.1021/es050795f>.
- [23] Huijgen WJJ, Witkamp GJ, Comans RNJ. Mechanisms of aqueous wollastonite carbonation as a possible CO₂ sequestration process. *Chem Eng Sci* 2006;61: 4242–51. <https://doi.org/10.1016/j.ces.2006.01.048>.
- [24] Hu J, Liu W, Wang L, Liu Q, Chen F, Yue H, et al. Indirect mineral carbonation of blast furnace slag with (NH₄)₂SO₄ as a recyclable extractant. *Journal of Energy Chemistry* 2017;26:927–35. <https://doi.org/10.1016/j.jchem.2017.06.009>.
- [25] International Energy Agency (2021): Net Zero by 2050 A Roadmap for the Global Energy Sector <https://www.iea.org/reports/net-zero-by-2050>.
- [26] International Organization for Standardization. (2020): Particle size analysis — Laser diffraction methods (ISO/DIS Standard No. 13320). Retrieved from: <https://www.iso.org/standard/69111.html>.
- [27] Kaliyavaradhan SK, Ling TC. Potential of CO₂ sequestration through construction and demolition (C&D) waste—An overview. *Journal of CO₂ Utilization* 2017;20: 234–42. <https://doi.org/10.1016/j.jcou.2017.05.014>.
- [28] Kodama S, Nishimoto T, Yamamoto N, Yogo K, Yamada K. Development of a new pH-swing CO₂ mineralization process with a recyclable reaction solution. *Energy* 2008;33:776–84. <https://doi.org/10.1016/j.energy.2008.01.005>.
- [29] Lackner KS, Wendt CH, Butt DP, Joyce Jr EL, Sharp DH. Carbon dioxide disposal in carbonate minerals. *Energy* 1995;20:1153–70. [https://doi.org/10.1016/0360-5442\(95\)00071-N](https://doi.org/10.1016/0360-5442(95)00071-N).
- [30] Lekakh SN, Rawlins CH, Robertson DGC, Richards VL, Peaslee KD. Kinetics of Aqueous Leaching and Carbonization of Steelmaking Slag. *Metallurgical and Materials Transactions* 2008;39:125–34. <https://doi.org/10.1007/s11663-007-9112-8>.
- [31] Li H, Tang Z, Li N, Cui L, Mao X. Mechanism and process study on steel slag enhancement for CO₂ capture by seawater. *Appl Energy* 2020;276:115515. <https://doi.org/10.1016/j.apenergy.2020.115515>.
- [32] Liu W, Teng L, Rohani S, Qin Z, Zhao B, Xu CC, et al. CO₂ mineral carbonation using industrial solid wastes: A review of recent developments. *Chem Eng J* 2021; 416:129093. <https://doi.org/10.1016/j.cej.2021.105644>.
- [33] Levenspiel O. *Chemical Reaction Engineering*. John Wiley & Sons; United States of America; 1999. p. 378. ISBN 0-471-25424-X.
- [34] Mayes WM, Riley AL, Gomes HI, Brabham P, Hamlyn J, Pullin H, et al. Atmospheric CO₂ sequestration in iron and steel slag: Conssett, Co., Durham. UK Environmental Science & Technology 2018;52:7892–900. <https://doi.org/10.1021/acs.est.8b01883>.
- [35] M. Mazzotti, J.C. Abanades, R. Allam, K.S. Lackner, F. Meunier, E. Rubin, J. C. Sanchez, K. Yogo, R. Zevenhoven (2005) IPCC Special Report on Carbon dioxide Capture and Storage ISBN-13 978-0-521-86643-9.
- [36] R. Márkus (2011): Salakgranulátó technológia kialakítása az acélgártási salak építőipari hasznosítása elősegítésére. *Anyagok Világa*. ISSN:1586-0140.
- [37] Mendoza EYM, Santos AS, López EV, Drozd V, Durygin A, Chen J, et al. Siderite Formation by Mechanochemical and High Pressure-High Temperature Processes for CO₂ Capture Using Iron Ore as the Initial Sorbent. *Processes* 2019;7:735. <https://doi.org/10.3390/pr7100735>.
- [38] B. Metz, O. Davidson, H. de Coninck, M. Loos, L. Meyer (2018) Carbon Dioxide Capture and Storage. IPCC Special Report ISBN-13 978-0-521-86643-9.
- [39] M.J. Mitchell, O.E. Jensen, K.A. Cliffe, M.M. Maroto-Valer (2009): A model of carbon dioxide dissolution and mineral carbonation kinetics. *Proceedings of the Royal Society A: Mathematical, Physical and Engineering Sciences* Vol. 466 pp. 1265-1290 doi: 10.1098/rspa.2009.0349.
- [40] Mucsi G. A review on mechanical activation and mechanical alloying in stirred media mill. *Chem Eng Res Des* 2019;148:460–74. <https://doi.org/10.1016/j.cherd.2019.06.029>.
- [41] Mucsi G, Halyag N, Kurusta T, Kristály F. Control of Carbon Dioxide Sequestration by Mechanical Activation of Red Mud. *Waste Biomass Valoriz* 2021;12:6481–95. <https://doi.org/10.1007/s12649-021-01466-2>.
- [42] Neto JBF, Faria JOG, Fredericci C, Chotoli FF, Silva ANL, Ferraro BB, et al. Modification of Molten Steelmaking Slag for Cement Application. *Journal of Sustainable Metallurgy* 2016;2:13–27. <https://doi.org/10.1007/s40831-015-0031-7>.
- [43] M.G. Nyambura, G.W. Muger, P.L. Felicia and N.P. Gathura (2011): Carbonation of brine impacted fractionated coal fly ash: implications for CO₂ sequestration Vol. 92 pp. 655-664 .
- [44] Opoczky L. Fine grinding and agglomeration of silicates. *Powder Technol* 1977;17: 1–7. [https://doi.org/10.1016/0032-5910\(77\)85037-7](https://doi.org/10.1016/0032-5910(77)85037-7).
- [45] United States Geological Survey (2020): Iron and steel slag data sheet – mineral commodities summary 2020 (<https://pubs.usgs.gov/periodicals/mcs2020/mcs2020-iron-steel-slag.pdf>).
- [46] Pan S-Y, Chang EE, Chiang P-C. CO₂ Capture by Accelerated Carbonation of Alkaline Wastes: A Review on Its Principles and Applications. *Aerosol Air Qual Res* 2012;12(5):770–91.
- [47] Pokrovsky OS, Schott J. Processes at the magnesium-bearing carbonates/solution interface. II. kinetics and mechanism of magnesite dissolution. *Geochim Cosmochim Acta* 1999;63:881–97. [https://doi.org/10.1016/S0016-7037\(99\)00013-7](https://doi.org/10.1016/S0016-7037(99)00013-7).
- [48] Proctor DM, Fehling KA, Shay EC, Wittenborn JL, Green JJ, Avent C, et al. Physical and Chemical Characteristics of Blast Furnace, Basic Oxygen Furnace, and Electric Arc Furnace Steel Industry Slags 2000;34(8):1576–82.
- [49] Pullin H, Bray AW, Burke IT, Muir DD, Sapsford DJ, Mayes WM, et al. Atmospheric Carbon Capture Performance of Legacy Iron and Steel Waste. *Environ Sci Tech* 2019;53:9502–11. <https://doi.org/10.1021/acs.est.9b01265>.
- [50] Ren S, Aldahri T, Liu W, Liang B. CO₂ mineral sequestration by using blast furnace slag: From batch to continuous experiments. *Energy* 2021;214:118975. <https://doi.org/10.1016/j.energy.2020.118975>.
- [51] Rileya AL, MacDonald JM, Burke IT, Renforth P, Jarvis AP, Hudson-Edwards KA, et al. Legacy iron and steel wastes in the UK: Extent, resource potential, and management futures. *J Geochem Explor* 2020;219:106630. <https://doi.org/10.1016/j.jgexplo.2020.106630>.
- [52] Sahu RK, Patela RK, Ray BC. Neutralization of red mud using CO₂ sequestration cycle. *J Hazard Mater* 2010;179:28–34. <https://doi.org/10.1016/j.jhazmat.2010.02.052>.
- [53] Sanna A, Uibu M, Caramanna G, Kuusik R, Maroto-Valer MM. A review of mineral carbonation technologies to sequester CO₂. *Chem Soc Rev* 2014;43(23):8049–80.
- [54] Santos RM, Bouwel JV, Vandevelde E, Mertens G, Elesen J, Gervin TV. Accelerated mineral carbonation of stainless steel slags for CO₂ storage and waste valorization: Effect of process parameters on geochemical properties. *Int J Greenhouse Gas Control* 2013;17:32–45. <https://doi.org/10.1016/j.ijggc.2013.04.004>.
- [55] Saran RK, Kumar R, Yadav S. Climate change: mitigation strategy by various CO₂ sequestration methods. *International Journal of Advanced Research in Science. Engineering* 2017;6:299–308. ISBN:978-93-86171-17-7.
- [56] Schollbach K, Ahmed MJ, van der Laan SR. The mineralogy of air granulated converter slag. *International Journal of Ceramic Engineering & Science* 2020;3: 21–36. <https://doi.org/10.1002/ces2.10074>.
- [57] Seonhye L, Ji-Whan K, Soochun C, Jun-Hwan B, Seung-Woo L. CO₂ sequestration technology through mineral carbonation: An extraction and carbonation of blast slag. *Journal of CO₂ Utilization* 2016;16:336–45. <https://doi.org/10.1016/j.jcou.2016.09.003>.

- [58] Sipilä J, Teir S, Zevenhoven R. Carbon dioxide sequestration by mineral carbonation – Literature review update 2005–2007. Åbo Akademi University, Faculty of Technology, Heat Engineering Laboratory; 2008. Report VT 2008–1..
- [59] Gopinath S, Mehra A. Carbon dioxide sequestration using steel slag modeling and experimental investigation. In: Carbon Dioxide Sequestration in Cementitious Construction Materials. Elsevier; 2018. p. 65–80.
- [60] Soong Y, Fauth DL, Howard BH, Jones JR, Harrison DK, Goodman AL, et al. CO₂ sequestration with brine solution and fly ashes. *Energ Conver Manage* 2006;47: 1676–85. <https://doi.org/10.1016/j.enconman.2005.10.021>.
- [61] Stanienda-Pilecki KJ. Magnesium calcite in Muschelkalk limestones of the Polish part of the Germanic Basin. *Carbonates Evaporites* 2018;33:801–21. <https://doi.org/10.1007/s13146-018-0437-y>.
- [62] Stolaroff JK, Lowry GV, Keith DW. Using CaO- and MgO-rich industrial waste streams for carbon sequestration. *Energ Conver Manage* 2005;46:687–99. <https://doi.org/10.1016/j.enconman.2004.05.009>.
- [63] Sun Y, Yao MS, Zhang JP, Yanga G. Indirect CO₂ mineral sequestration by steelmaking slag with NH₄Cl as leaching solution. *Chem Eng J* 2011;173:437–45. <https://doi.org/10.1016/j.cej.2011.08.002>.
- [64] Sverjensky DA, Sahai N. Theoretical prediction of single-site surface-protonation equilibrium constants for oxides and silicates in water. *Geochim Cosmochim Acta* 1996;60(20):3773–97.
- [65] Tian S, Jiang J, Chen X, Yan F, Li K. Direct Gas-Solid Carbonation Kinetics of Steel Slag and the Contribution to In situ Sequestration of Flue Gas CO₂ in Steel-Making Plants. *ChemSusChem* 2013;6:2348–55. <https://doi.org/10.1002/cssc.201300436>.
- [66] Turvey CC, Wilson SA, Hamilton JL, Tait AW, McCutcheon J, Beinlich A, et al. Hydrotalcites and hydrated Mg-carbonates as carbon sinks in serpentinite mineral wastes from the Woodsreef chrysotile mine, New South Wales, Australia: Controls on carbonate mineralogy and efficiency of CO₂ air capture in mine tailings. *Int J Greenhouse Gas Control* 2018;79:38–60. <https://doi.org/10.1016/j.ijggc.2018.09.015>.
- [67] Udvardi B, Géber R, Kocserha I. Aktualitások az úépítésben hasznosítható másodlagos nyersanyagok területén. Aktualitások az úépítésben hasznosítható másodlagos nyersanyagok területén Ütögyi Lapok: A Közlekedésépítési Szakterület Mérnöki és Tudományos Folyóirata 2019;7(12):33–41.
- [68] Ukwattage NL, Ranjith PG, Wang SH. Investigation of the potential of coal combustion fly ash for mineral sequestration of CO₂ by accelerated carbonation. *Energy* 2013;52:230–6. <https://doi.org/10.1016/j.energy.2012.12.048>.
- [69] Uliasz-Bocheńczyk A, Mokrzycki E, Piotrowski Z, Pomykała R. Estimation of CO₂ sequestration potential via mineral carbonation in fly ash from lignite combustion in Poland. *Energy Procedia* 2009;1:873–4879. <https://doi.org/10.1016/j.egypro.2009.02.316>.
- [70] Wang L, Liu W, Hu J, Liu Q, Yue H, Liang B, et al. Indirect mineral carbonation of titanium-bearing blast furnace slag coupled with recovery of TiO₂ and Al₂O₃. *Chin J Chem Eng* 2018;26:583–92. <https://doi.org/10.1016/j.cjche.2017.06.012>.
- [71] Wei C, Dong J, Zhang H, Wang X. Kinetics model adaptability analysis of CO₂ sequestration process utilizing steelmaking slag and cold-rolling wastewater. *J Hazard Mater* 2021;404:124094. <https://doi.org/10.1016/j.jhazmat.2020.124094>.
- [72] De Windt L, Chaurand P, Rose J. Kinetics of steel slag leaching: Batch tests and modeling. *Waste Manag* 2011;31(2):225–35.
- [73] Xu T, Apps JA, Pruess K. Mineral sequestration of carbon dioxide in a sandstone–shale system. *Chem Geol* 2005;217:295–318. <https://doi.org/10.1016/j.chemgeo.2004.12.015>.
- [74] Xu T, Apps JA, Pruess K. Numerical simulation of CO₂ disposal by mineral trapping in deep aquifers. *Appl Geochem* 2014;19:917–36. <https://doi.org/10.1016/j.apgeochem.2003.11.003>.
- [75] Yadav VS, Prasad M, Khan J, Amritphale SS, Singh M, Raju CB. Sequestration of carbon dioxide (CO₂) using red mud. *J Hazard Mater* 2010;176:1044–50. <https://doi.org/10.1016/j.jhazmat.2009.11.146>.
- [76] Yadav VS, Mehra A. Experimental study of dissolution of minerals and CO₂ sequestration in steel slag. *Waste Manag* 2017;64:348–57. <https://doi.org/10.1016/j.wasman.2017.03.032>.
- [77] R. Zevenhoven, A. B. Mukherjee, T. Koljonen, J. Kohlman (2002): Mineral carbonation for long-term storage of CO₂ from flue gases: Final report for Finnish national research programme CLIMTECH (1999–2002). Helsinki University of Technology ISSN: 1457-9944.
- [78] Zhang H, Wei C, Dong J. Inhibition Kinetics of Chromium Leaching by Calcite Coating on the Surface of Stainless Steel Slag via the Gas-Solid Accelerated Carbonation Process. *Waste Biomass Valoriz* 2021;12:475–85. <https://doi.org/10.1007/s12649-020-00988-5>.

Further reading

- [13] Eloneva S, Teir S, Salminen J, Fogelholm CJ, Zevenhoven R. Fixation of CO₂ by carbonating calcium derived from blast furnace slag. *Energy* 2008;33:1461–97. <https://doi.org/10.1016/j.energy.2008.05.003>.